International Journal of Thermophysics, Vol. 26, No. 2, March 2005 (© 2005)
DOI: 10.1007/s10765-005-4515-8

Characterization of the Pore Structure of Ceramics via Propagation of Light and Infrared Radiation[1]

J. Manara,[2,3] R. Caps,[4] and J. Fricke[2]

The pore size distributions of alumina and magnesia ceramics were determined by measuring the directional-hemispherical transmittance and reflectance. These values are highly sensitive to changes of the pore structure. The partially sintered alumina samples were measured at room temperature in a wavelength range from 0.5 to 6 μm. The equation of radiative transfer can be solved for absorbing and scattering media by a three-flux solution. With this three-flux solution the scattering coefficients were derived from the measured directional-hemispherical transmittance and reflectance. The scattering coefficients can also be calculated theoretically by the Mie theory, if the pore size distribution is known. Finally, the quantitative pore size distribution was determined by fitting the theoretical scattering coefficients to the experimental scattering coefficients. To check the correctness of the derived pore-size distribution, scanning electron microscopy (SEM) and atomic force microscopy (AFM) pictures of the alumina samples were taken. The pore-size distribution was then derived by counting the pores and determining the diameters D of the spherical pores. Both results agree well and show that the new procedure is a valuable tool to extract structural information during the final sintering state.

KEY WORDS: ceramics; diffuse transmission; Mie theory; pore-size distribution; radiative transfer; three-flux approximation.

[1]Paper presented at the Sixteenth European Conference on Thermophysical Properties, September 1–4, 2002, London, United Kingdom.

[2]Bavarian Center for Applied Energy Research (ZAE Bayern), Am Hubland, D-97074 Würzburg, Germany.
[3]To whom correspondence should be addressed. E-mail: manara@zae.uni-wuerzburg.de
[4]va-Q-tec AG, Karl-Ferdinand-Braun-Str. 7, D-97080 Würzburg, Germany.

1. INTRODUCTION

Ceramics are usually produced via sintering at high temperatures. The properties of the resulting material depend on the sintering parameters, like sintering temperature, sintering time, cooling and heating rates, and sintering atmosphere in the furnace. Thus, for different raw materials and applications adapted sintering conditions are necessary [1]. An empirical optimization of the sintering conditions is expensive, as the sintering process is influenced by many parameters. Therefore, new methods are desirable that can be used to extract results *in situ*, during the sintering process.

Until now, changes of the microstructure of the material during sintering were detected by measuring the shrinkage of the material via dilatometry. This method can be used to determine the pore volume which is an important parameter for the sintering process. Dilatometry is a difference method, which depends on the exact determination of the density before or after sintering. The sensitivity of dilatometry decreases strongly towards the end of sintering, when shrinkage ceases. The sintering process is most interesting at this state, however. If sintering is stopped too early, the mechanical properties may be poor, because of still existing pores. If the sintering takes too long, the mechanical strength may be reduced, because unwanted grain growth had occurred. To get optimal mechanical properties, the sintering has to be stopped at a certain point.

Scattering of light and infrared radiation has been introduced as an additional method for detecting changes in porosity [2–4]. The radiation is mainly scattered at the pore-particle interfaces. Although the variation of the total porosity decreases strongly towards the end of the sintering process, the variation of the pore-size distribution is still significant. As the scattering is influenced by both parameters, the transmittance is highly sensitive to the changes of the pore-size distribution during the final sintering state.

2. DETERMINATION OF SCATTERING COEFFICIENTS FROM THE DIRECTIONAL-HEMISPHERICAL TRANSMITTANCE AND REFLECTANCE

In this section the equation of radiative transfer is solved for scattering and absorbing media. As a result one gets the directional-hemispherical transmittance T_{dh} and reflectance R_{dh} and their dependence on the optical thickness τ_0 and the albedo $\omega_0 = S/E$, which gives the contribution of scattering to the extinction. Here, only a short summary of the theoretical background is given. A more detailed description of this theory can be found in Refs. [5] and [6].

2.1. Radiative Transport in Porous Media

The change of light intensity is described by the equation of radiative transfer [7]:

$$\mu \frac{\mathrm{d}I(\tau)}{\mathrm{d}\tau} = -I(\tau) + \frac{\omega_0}{4\pi} \int_{4\pi} I(\tau, \Omega') p(\tau, \Omega', \Omega) \mathrm{d}\Omega' + J(\tau). \tag{1}$$

The following symbols are used in Eq. (1): $I(\tau)$ is intensity at optical depth τ, $\mu = \cos\theta$ is direction cosine, ω_0 is albedo, $p(\tau, \Omega', \Omega)$ is phase function for the radiation that is coming from the solid angle Ω' and is scattered into the solid angle Ω, and $J(\tau)$ is source term. The source term accounts for the incoming radiation F, that reaches the point τ [7]:

$$J(\tau) = \frac{\omega_0 F}{4\pi} \rho_\mathrm{p}(\tau) = \frac{\omega_0 F}{4\pi} \frac{1 - R_\mathrm{p}}{1 - R_\mathrm{p}^2 \exp(-2\tau_0)} \left[\exp(-\tau) + R_\mathrm{p} \exp(-2\tau_0 + \tau)\right]. \tag{2}$$

$\rho_\mathrm{p}(\tau)$ is calculated under consideration of multiple reflections at the surfaces of the sample, where R_p is the reflectance perpendicular to the surface (normal-normal reflectance) [8].

As we consider only cold samples, the emission term is omitted in Eq. (1).

2.2. Solution of the Equation of Radiative Transfer

The integral of the scattering source term in Eq. (1) can be changed into a sum over a few intensities (discrete ordinate method). Consideration of three discrete directions leads to the three-flux solution. Finally, the directional-hemispherical transmittance T_dh and reflectance R_dh can be calculated as a function of the intensity inside the sample [9]:

$$T_\mathrm{dh} = \frac{\left(1 - \bar{R}_\mathrm{i}\right) I_{+1}(\tau^* = \tau_0^*, \omega_0^*) + \frac{F}{\pi} \frac{(1 - R_\mathrm{p})^2}{1 - R_\mathrm{p}^2 \exp(-2\tau_0^*)} \exp\left(-\tau_0^*\right)}{\frac{F}{\pi}}, \tag{3}$$

$$R_\mathrm{dh} = \frac{\left(1 - \bar{R}_\mathrm{i}\right) I_{-1}(\tau^* = 0, \omega_0^*) + \frac{F}{\pi} R_\mathrm{p} + \frac{F}{\pi} \frac{(1 - R_\mathrm{p})^2 R_\mathrm{p} \exp(-2\tau_0^*)}{1 - R_\mathrm{p}^2 \exp(-2\tau_0^*)}}{\frac{F}{\pi}}. \tag{4}$$

It is possible to define the mean internal reflectance $\bar{R}_\mathrm{i}$ by

$$\bar{R}_\mathrm{i}(m, k) = \frac{\int_0^1 \mu R_\mathrm{i}(\mu, m, k) \mathrm{d}\mu}{\int_0^1 \mu \mathrm{d}\mu} = 2 \int_0^1 \mu R_\mathrm{i}(\mu, m, k) \mathrm{d}\mu, \tag{5}$$

where R_i is the angular dependent internal reflectance, and m is the real part and k is the imaginary part of the complex refractive index $n = m - ik$.

The effective values can be calculated using the anisotropy factor g [10]:

$$\tau^* = \tau\,(1 - \omega_0 g)\ ,\ \omega_0^* = \frac{\omega_0\,(1-g)}{1-\omega_0 g}. \tag{6}$$

The values of the anisotropy factor g are within the interval -1 (backward scattering) to $+1$ (delta function like forward scattering). By measuring the directional-hemispherical transmittance, one gets the effective optical thickness and the effective albedo. The directional-hemispherical transmittance includes the diffuse transmittance as well as the direct non-scattered beam (in-line transmission). This allows coverage of a porosity range between 0.1% and 5%, which is important for applications. Until now, usually highly dense ceramics with a porosity below 0.5% have been investigated [2–4]; as in most cases, only the directly transmitted beam (in-line), which decays exponentially with sample thickness, was measured. So one gets a relationship between the effective optical thickness τ_0^* and the effective albedo ω_0^* on one side and the directional-hemispherical transmittance T_{dh} and reflectance R_{dh} on the other side.

2.3. Calculation of the Pore Sizes

The spectral variation of the effective scattering coefficient S^* is influenced by the pore structure of the ceramic, i.e., the size, shape, and porosity Π of the sample. The effective relative scattering cross section Q^* of the pores and therefore the effective scattering coefficient S^* can be calculated by the Mie theory as shown in Ref. 5:

$$S^*(\lambda) = \frac{3}{2}\Pi\frac{Q^*(\lambda)}{D}. \tag{7}$$

Here we assume that the pore volume within a logarithmic diameter interval $\Delta \ln D$ is distributed like a logarithmic normal distribution, as is mostly the case [11]:

$$f(d)\,\Delta \ln D = \frac{1}{\sqrt{2\pi}\,\sigma_g}\exp\left[-\frac{(\ln D - \ln D_M)^2}{2\sigma_g^2}\right]\Delta \ln D. \tag{8}$$

By a least-squares fit with the measured spectral effective scattering coefficient S^*_{exp} and the spectral effective scattering coefficient S^* calculated from Eq. (7), the modal value D_M and the geometric mean standard deviation σ_g can be calculated.

3. SAMPLE PRODUCTION AND EXPERIMENTAL SET UP

The measured samples are derived from highly pure Al_2O_3- and MgO- powder. The alumina samples were produced by the Fraunhofer-Institut für Silicatforschung (ISC) and the magnesia samples were produced by the ZAE Bayern as follows. First, the powder was filled into a cylindrical silicone vessel ($\oslash_{\text{inside}} = 22\,\text{mm}$, length = 30 mm). The silicone vessel was compressed isostatically at 250 MPa for 15 min. The green body were then sintered at different temperatures. For light scattering measurements the cylindrical ceramic sample was cut into plane-parallel slices with a diamond saw.

The directional-hemispherical transmittance T_{dh} of both the diffusely scattered radiation and the transmitted direct beam through the sample was measured by an integrating sphere [12]. Also determined was the directional-hemispherical reflectance R_{dh} of the diffusely scattered radiation and the direct beam, which is reflected at the surface. For the wavelength range from 0.25 to 2.5 μm, a Perkin Elmer lambda 9 spectrometer was used, and for the wavelength range from 2.5 to 18 μm, a Bruker IFS 66v FTIR-spectrometer was employed.

4. RESULTS AND ANALYSIS

First, the directional-hemispherical transmittance and reflectance of all produced samples were measured. As an example, the directional-hemispherical transmittance T_{dh} and reflectance R_{dh} are shown in Fig. 1 for a group of samples sintered at the same conditions. Measurements were done for four different thicknesses d. The transmittance decreases with increasing sample thickness, because the optical thickness increases with increasing sample thickness. The reflectance increases with increasing sample thickness due to backward scattering. Below 0.3 μm and between 6 and 11 μm, absorption is dominant. This dependence is similar for all prepared groups of samples. The absorption peaks between 2.6 and 3.6 μm and the small peak at 4.3 μm are due to atmospheric water and carbon dioxide, respectively.

From the directional-hemispherical transmittance and reflectance the effective optical thickness and the effective albedo or the effective scattering coefficient and the effective albedo, respectively, were calculated for all samples using Eqs. (3) and (4). The resulting effective scattering coefficient S^* is depicted in Fig. 2 for the same group of samples shown in Fig. 1. As all samples of one group are sintered together at the same conditions, the scattering coefficient has to be equal for all samples of one group. As can be seen from Fig. 2 this is the case in the wavelength range from 0.5 to 6 μm. Below 0.5 μm and above 6 μm this is not the case due to the low

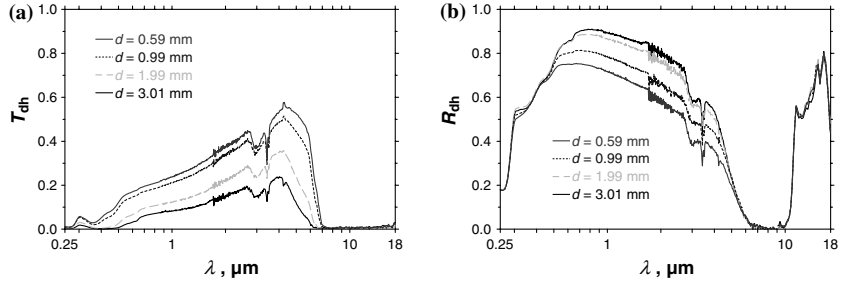

Fig. 1. Dependence of the (a) directional-hemispherical transmittance T_{dh} and (b) reflectance R_{dh} on the wavelength λ from 0.25 to 18 μm for a group of samples with different thicknesses d sintered at the same conditions. The samples are first sintered at 1273 K for 24 h and then at 1888 K for 1 h. The resulting porosity is $\Pi = 2.08\%$.

transmittance of the samples. Equations (3) and (4) only provide reliable results if the directional-hemispherical transmittance lies between 0.1 and 0.6. Therefore, only the wavelength range from 0.5 to 6 μm was used for determining the pore structure of the samples.

The same procedure was carried out with ten different groups of samples. Every group of samples was sintered at the same conditions. The pore volume distribution of every group of samples was determined by a least-squares fit. As shown in Fig. 3 for three groups, the measured effective scattering coefficient S^*_{exp} and the fitted effective scattering coefficient

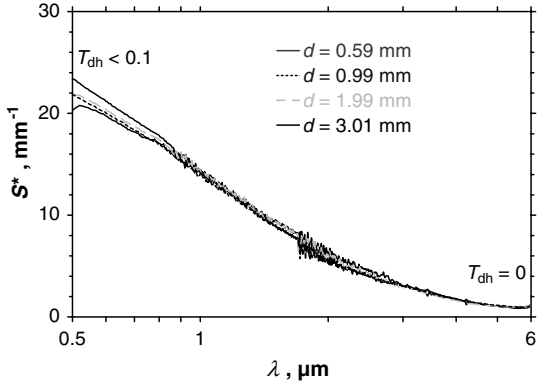

Fig. 2. Dependence of the effective scattering coefficient S^* on the wavelength λ. Between 0.5 and 6 μm the scattering coefficient is equal for the four samples with different thicknesses d.

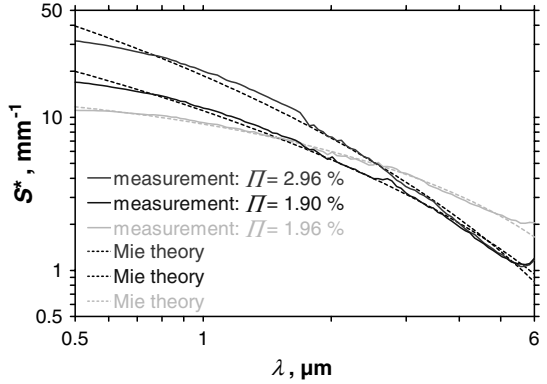

Fig. 3. Measured effective scattering coefficient S^*_{exp} (solid lines) and calculated effective scattering coefficient S^* (doted lines) for three groups of samples, sintered under different conditions.

S^* are very similar. The effective scattering coefficient S^* was calculated by varying the modal value D_M and the geometric mean standard deviation σ_g of the pore size distribution.

The resulting pore volume distributions and the sintering conditions of all ten groups of samples are depicted in Table I. The sintering temperature varies from $T = 1845$ to 1923 K and the sintering time t is 1 or 24 h. The first five groups are prepared without pre-sintering, whereas the second five groups received a pre-sintering. Pre-sintering means that the samples are first sintered for 24 h at 1273 K and, after that, the samples are sintered at the conditions given in Table I. The three samples shown in Fig. 3 are identified in Table I. Obviously the modal value of the pore

Table I. Sintering Conditions and Resulting Pore Volume Distributions for 10 Investigated Groups of Al_2O_3 Samples

Sintering temperature and time		Without pre-sintering			With pre-sintering		
T (K)	t (h)	Π(%)	D_M (µm)	σ_g	Π(%)	D_M (µm)	σ_g
1845	1	3.14	0.21	1.59	2.96	0.28	1.45
1888	1	1.96	0.67	1.54	2.08	0.37	1.51
1927	1	1.62	1.04	1.53	1.90	0.68	1.71
1963	1	1.34	1.18	1.05	1.55	1.30	1.37
1923	24	2.36	2.29	1.15	1.96	2.23	1.22

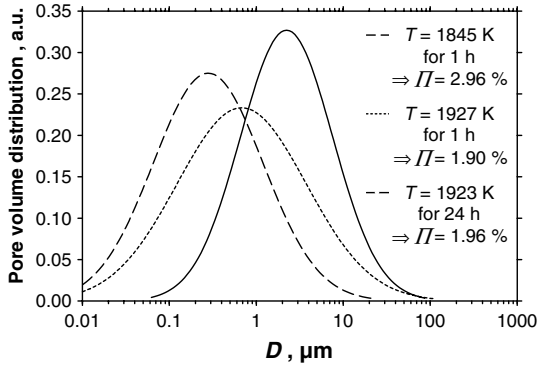

Fig. 4. Pore volume distribution of three groups of samples, which are sintered under different conditions. The maximum of the curve is given by the modal value D_M, and the width of the curve is characterized by the geometric mean standard deviation σ_g. Although the porosity Π is similar, the pore volume distribution differs significantly.

volume distribution increases with increasing sintering time and temperature. The pore volume distribution is shown in Fig. 4 for the three groups of samples identified in Table I. The pore volume distribution differs significantly, although the porosity of the samples is similar.

To check the correctness of the derived pore size distributions, SEM and AFM pictures of the alumina samples were taken. The pore size distribution was then derived by counting the pores and determining the diameters D of the spherical pores.

In Fig. 5(a) SEM picture of an alumina sample, which has first been sintered at 1273 K for 24 h and then at 1923 K for an additional 24 h is shown. The average pore size derived from the SEM pictures for this sample is about 2 µm, which is in accordance with the result depicted in Fig. 4 (solid line). As the SEM pictures are not sensitive enough for smaller pore sizes, AFM pictures are made to verify the whole range of the pore size distribution. In Fig. 6 an AFM picture of an alumina sample, which first has been sintered at 1273 K for 24 h and then at 1845 K for 1 h can be seen. The average pore size derived from the AFM pictures for this sample is about 0.28 µm, which is very similar to the result depicted in Fig. 4 (dashed line). Both results agree well and show that the new procedure is a valuable tool to extract structural information during the final sintering state.

Finally the same measurements and analysis were done with two groups of magnesia samples to make a transfer to another material. The

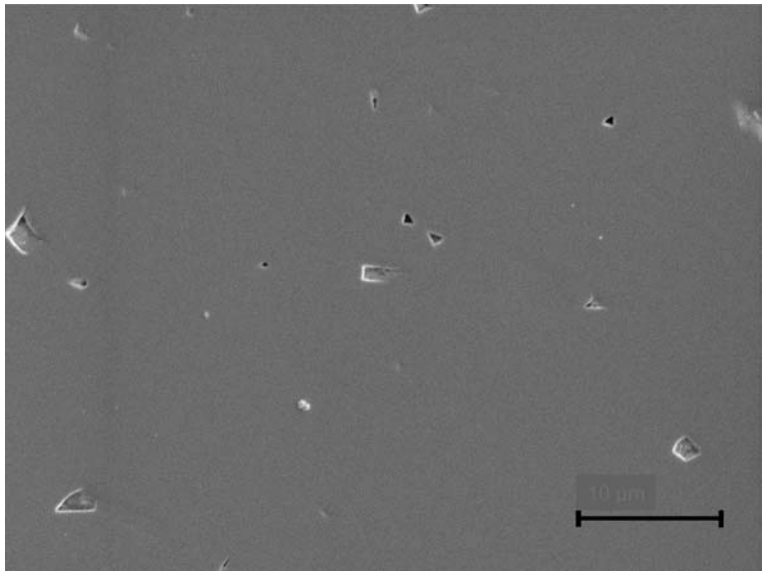

Fig. 5. SEM picture of an Al_2O_3 sample, which has first been sintered at 1273 K for 24 h and then at 1923 K for an additional 24 h. The average pore size derived from the SEM pictures for this sample is about 2 µm, which is very similar to the result derived from scattering of light and infrared radiation (solid line in Fig. 4).

results are depicted in Table II. Here a different effect can be seen. Whereas for the alumina samples where the average pore size increases with increasing sintering temperature and time, the pore size within the magnesia sample decreases with increasing sintering time.

This can be explained easily. In the early and middle states of sintering, the porosity decreases with increasing sintering time, and with the decrease of porosity, the pore size also decreases [13]. The magnesia samples depicted in Table II are still in the middle stage of sintering. But in the last stage of sintering the decrease of porosity ceases. Now the average pore size increases with increasing sintering time, because several small pores combine to one bigger pore, without changing the porosity, which is energetically more favorable [14].

5. CONCLUSIONS

The analysis carried out at ZAE Bayern has shown that it is possible to determine the pore structure of ceramics by measuring the spectral variation of the directional-hemispherical transmittance and reflectance. This

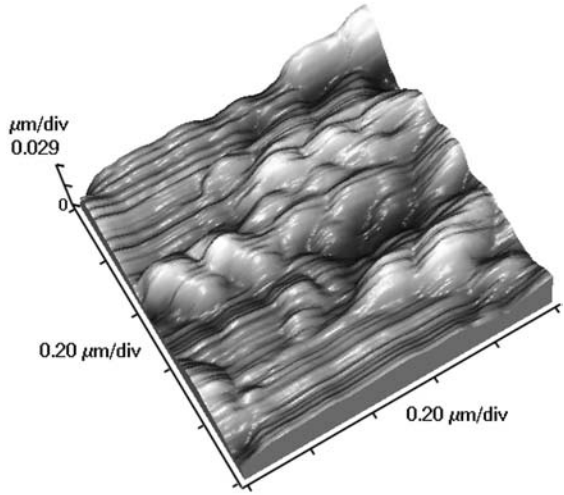

Fig. 6. AFM picture of an Al_2O_3 sample, which has first been sintered at 1273 K for 24 h and then at 1845 K for 1 h. The average pore size derived from the AFM pictures for this sample is about 0.28 μm, which is very similar to the result derived from scattering of light and infrared radiation (dashed line in Fig. 4).

Table II. Sintering Conditions and Resulting Pore Volume Distributions for Two Investigated Groups of MgO Samples

T (K)	t (h)	Π (%)	D_M (μm)	σ_g
1500	1	9.05	2.10	0.92
1500	5	5.15	1.04	1.06

can be done for different absorbing and scattering media. In this paper we verified this method for alumina and magnesia ceramics. But, in general, this method should be applicable to other ceramic materials.

ACKNOWLEDGMENT

This work was supported by the German Science Foundation (DFG, grant number CA196/1-1) Bonn.

NOMENCLATURE

ω_0	albedo
g	anisotropy factor
θ	angle relative to the surface normal
n	complex refractive index
$D, \oslash$	diameter
μ	direction cosine
R_{dh}	directional-hemispherical reflectance
T_{dh}	directional-hemispherical transmittance
E	extinction coefficient
σ_g	geometric mean standard deviation
k	imaginary part of the complex refractive index
I, J	intensity
$\bar{R}_{\mathrm{i}}$	mean internal reflectance
D_{M}	modal value
τ	optical depth
τ_0	optical thicks
p	phase function
Π	porosity
F	radiative flux
m	real part of the complex refractive index
R_{p}	reflection of perpendicular beam onto surface
Q	relative scattering cross section
S	scattering coefficient
Ω	solid angle
T	temperature
d	thickness
λ	wavelength
Superscript *	effective

REFERENCES

1. F. Thümmler, *Pulvermetallurgie in Wissenschaft und Praxis* **5**:261 (1989).
2. W. W. Chen and B. J. Dunn, *J. Am. Ceram. Soc*. **76**:2083 (1993).
3. J. G. J. Peelen and R. Metselaar, *J. Appl. Phys*. **45**:216 (1974).
4. R. Hanna, *J. Am. Ceram. Soc*. **48**:376 (1965).
5. C. F. Bohren and D. R. Huffmann, *Absorption and Scattering of Light by Small Particles* (John Wiley, New York, 1983).
6. T. Burger, Dissertation (Universität Würzburg, 1998).
7. J. Manara, R. Caps, F. Raether and J. Fricke, *Optics Commun*. **168**:237 (1999).
8. E. Hecht, *Optics* (Addison-Wesley, New York, 1987).
9. J. Manara, Dissertation (Universität Würzburg, 2001).

10. B. H. J. McKellar and M. A. Box, *J. Atmos. Sci*. **38**:1063 (1981).
11. M. Kerker, *The Scattering of Light and Other Electromagnetic Radiation* (Academic Press, Orlando, Florida, 1969).
12. T. Burger, J. Kuhn, R. Caps and J. Fricke, *Appl. Spectrosc*. **51**:309 (1997).
13. R. M. German, *Sintering Theory and Practice* (John Wiley, New York, 1996).
14. W. Schatt, *Sintervorgänge – Grundlagen* (VDI-Verlag, Düsseldorf, 1992).